Journal of Materials Research and Technology 36 (2025) 3436–3450

Contents lists available at ScienceDirect

Journal of Materials Research and Technology

journal homepage: www.elsevier.com/locate/jmrt

Tribological performance of different alloyed DLC and AlTiSiN coatings when sliding against Inconel 718 alloy for demanding applications

Cristian Pérez-Salinas [a,b,*], Filipe Fernandes [c,d,**], Manuel Evaristo [c], Albano Cavaleiro [c], Ch Sateesh Kumar [c,f], L. Norberto López de Lacalle [b,e]

[a] Universidad Técnica de Ambato, Faculty of Civil and Mechanical Engineering, Ambato, Ecuador
[b] Department of Mechanical Engineering, ESI Bilbao, University of the Basque Country, Bilbao, Spain
[c] University of Coimbra, CEMMPRE, ARISE, Department of Mechanical Engineering, Coimbra, Portugal
[d] CIDEM, ISEP - Polytechnic of Porto, Rua Dr. António Bernardino de Almeida, 4249-015, Porto, Portugal
[e] Aeronautics Advanced Manufacturing Centre (CFAA), University of the Basque Country (UPV/EHU), Bizkaia Technology Park -Ed.202, 480170, Zamudio, Spain
[f] Laboratory for Tribology and Interface Nanotechnolcogy, Faculty of Mechanical Engineering, University of Ljubljana, Askerceva 6, 1000, Ljubljana, Slovenia

ARTICLE INFO

Handling editor: P Rios

Keywords:
Reciprocating sliding test
DLC alloyed films
AlTiSiN coating
Tribological properties
Inconel 718

ABSTRACT

Machining Ni alloys such as Inconel 718 is challenging due to its good mechanical properties, low thermal conductivity and low elastic modulus, which causes high cutting temperatures at the chip-tool interface. The use of self-lubricating coatings, such as DLCs coatings has potential to improve significantly the machinability of Ni alloys. This research work aims to explore how different DLC, DLC-Si, DLC-W coatings behave tribologically when sliding against Inconel 718. The results will be compared with an industrial AlTiSiN coating used to protect the cutting tools. The morphology, mechanical properties and chemical composition of the coatings were analysed. To evaluate the tribological behaviour alternative sliding tests were performed under different conditions (room temperature – RT and 200 °C in dry condition and at RT with lubrication, using CUT-MAX S 50259-1 oil. The DLC coatings showed remarkable self-lubricating efficiency, with low coefficients of friction even in dry conditions, demonstrating that their self-lubricating capability is effective without the need for external lubricants. However, at a temperature of 200 °C, a significant increase in wear rate was observed for all DLC coatings, being 3 to 4 times higher as compared to that at room temperature. This is mainly caused by the conversion of sp^3 to sp^2 bonds coating oxidation. On the other hand, AlTiSiN demonstrated consistent specific wear rate, despite of the unfavourable circumstances, highlighting its suitability to use in extreme environments. These results show the limitations in film performance and underline the importance of balancing the strength of the coating with its impact on the opposing surface. Furthermore, it highlights the need to improve the thermal stability of DLC coatings for application in high temperature environments and dry conditions.

1. Introduction

Dry machining of nickel alloys has gained prominence due to the ecological risks of metallurgical fluids and the increasing focus on sustainability. This strategy reduces the carbon footprint of manufacturing processes [1], but it presents challenges, such as rapid tool wear caused by high stresses and temperatures. Tungsten carbide (WC) is proving to be a predominant cutting material for nickel alloys in high-speed broaching, as it enables higher material removal rates than high speed steel - *HSS* [2]. However, it suffers from accelerated wear due to abrasive and adhesive mechanisms, as well as Co diffusion/loss [3]. Although ceramic tools offer greater wear resistance at high speeds, their high cost and brittleness limit their use [4,5]. In low-speed processes, such as broaching, where temperature is moderate, diamond-like carbon (DLC) coatings can be a viable alternative to protect the surface of the tools due to their self-lubricating properties, which reduce friction and minimize thermal rise. This makes them a promising option for dry and near-dry machining, promoting sustainability in manufacturing [6].

The growing interest in improving productivity and sustainability has driven the development of more efficient coatings. DLC coatings stand out for their high hardness, low friction coefficient, and excellent wear resistance, which reduces machining forces during cutting. This

* Corresponding author. Universidad Técnica de Ambato, Faculty of Civil and Mechanical Engineering, Ambato, Ecuador.
** Corresponding author. University of Coimbra, CEMMPRE, ARISE, Department of Mechanical Engineering, Coimbra, Portugal.
E-mail addresses: cperez072@ikasle.ehu.eus (C. Pérez-Salinas), fid@isep.ipp.pt (F. Fernandes).

https://doi.org/10.1016/j.jmrt.2025.03.269
Received 19 February 2025; Received in revised form 25 March 2025; Accepted 28 March 2025
Available online 3 April 2025

positive effect was demonstrated when machining aluminum alloys and aerospace composites [7,8]. Their tribological behavior varies depending on the type of counterpart which they interact with [9]. Similarly, tribological performance heavily depends on the contact environment, structure, and mechanical properties of the coating. Despite the extensive research on DLC sliding against steel and ceramics [10,11], no studies have been reported its interaction against nickel alloys as a counterpart. Recently, in the work of Khan et al. [12], it was reported that coatings deposited by *HiPIMS* (DLC-Ar, DLC-Ne) and arc (DLC-Bn) exhibited low friction and minimal wear against a titanium countersurface when subjected to loads of 10–20 N, however, their interaction with nickel alloys remains largely unexplored. Understanding this interaction is crucial to optimizing its functionality and ensuring its reliability in industrial applications.

Non-hydrogenated DLC coatings have an amorphous structure with sp^2 (graphitic) and sp^3 (diamond) carbon-carbon bonds. The ratio between sp3 and sp2 is important and defines their tribological properties [13]. The sp^3 bonds confer high hardness and wear resistance, while the sp^2 bonds promote self-lubrication [14–16]. However, their thermal stability is limited, as high temperatures induce graphitization and mechanical degradation [17]. To improve their high temperature properties, the DLC coatings were doped with elements such as Ti, Cr, Co, Ni, Al, Si and W, which modifies internal stress, thermal stability and wear resistance [6]. Studies have shown that W improves wear resistance at high temperatures (400–500 °C) [18] while Si increases hardness and thermal stability up to 500 °C [19]. These improvements are essential in sectors such as aerospace and automotive, where operating conditions are extreme. However, DLC coatings present challenges such as high internal compressive stress and low adhesion to metal substrates, which can lead to coatings delamination [20,21]. Previous studies have shown that the inclusion of a Cr interlayer improves adhesion to the substrate, which increases the durability of the coating [22,23].

The continuous development of high-performance materials, tools and components require the development of coatings with superior properties in terms of wear resistance, friction and thermal stability. Diamond-like carbon (DLC) films have emerged as an excellent option to reduce wear and friction in applications involving sliding contacts [13, 24–26]. These coatings stand out for their unique combination of properties, such as high hardness, low friction, and good chemical resistance. However, in high stress applications, like machining hard materials such as Inconel 718, their tribological behaviour and thermal stability require thorough evaluation. During machining of Inconel 718 at low speed (less than 30 m/min), temperatures closer to 300 °C can be easily reached [27], which can be considered as a critical condition to evaluate the efficiency of DLC coatings in such type of industrial applications.

While it is possible to synthesize DLC films with a wide range of mechanical and tribological properties, with or without the incorporation of doping elements [28,29], there is a lack of literature regarding the tribological behavior of these coatings when sliding against Inconel 718 alloy. This superalloy, known for its abrasive potential, poses significant challenges in machining processes, particularly at high temperatures generated by friction under high velocity sliding conditions. However, its interaction with DLC coatings at low velocities, such as those used in broaching processes, has been explored little, despite its potential for practical application. In view of this knowledge gap, the present study analyses the tribological performance of pure, Si and W doped DLC coatings c and a commercial AlTiSiN coating, which is widely used in protection of the surface of the cutting tools. For this purpose, alternative sliding tests were carried out against Inconel 718 under dry conditions (room temperature and 200 °C) and lubricated conditions. In addition, the structural and mechanical properties of the coatings were characterized to evaluate their potential for improving the machining of nickel alloys. The main objective of this work is to identify the wear mechanisms of different DLC coatings and to determine which one offers the best tribological performance in contact with Inconel 718, using an experimental reciprocating sliding configuration.

2. Materials and methods

2.1. Experimental set-up

The DLC type coatings of this work were deposited in a magnetron sputtering machine (UDP-650-4 Teer Coatings Ltd. UK) with a closed-field unbalanced magnetron sputtering system (CFUBMS) with different conditions as presented in Table 1. The targets are connected to DC power supplies, while for the substrates a pulsed DC was used. Four targets were used, two of carbon, one of chromium, one of silicon to alloy the films with Si and one of carbon with 14 pellets of tungsten with 20 mm integrated to deposit the W alloyed film. Argon (99.999 % purity) was used as working gas for establishing the plasma. On the other hand, a commercial AlTiSiN coatings used in the protection of cutting tools and supplied by the Metalestalki company was used for comparison proposes. This coating was produced in a PLATIT PL1401-Compact machine with *HiPIMS* technology at a higher deposition temperature than the DLC coatings. Since this coating belong to the portfolio of the Metalestalki enterprise, which underwent a long optimization process, the deposition conditions cannot be here disclosed, due to competitive reasons.

Samples of AISI M2 with mirror finishing were used as substrates with the final polishing process with 3 mm diamond paste. Silicon wafers were also used as substrates for mechanical and structural characterization of the coatings. M2 samples were used for the tribological characterization. Before placing the samples in the deposition, all substrates were ultrasonically cleaned in acetone and ethanol baths for 15 min and then air dried with dry air blowing.

Fig. 1 present a cross-section scheme of the deposition chamber with the arrangement of the targets: chromium, 2 carbon, and 1Si or carbon with W pellets. For all coatings, a chromium metallic adhesion layer with a thickness of 0.3–0.35 μm was deposited to improve the adhesion of the DLC-based coatings to the substrate. The DLC or Si-DLC coatings were deposited with a thickness in the range of 1.7–2.0 μm.

The deposition procedure starts with the evacuation of the chamber to a pressure lower than 10^{-3} Pa. Then, for each of the DLC, DLC-Si and DLC-W targets the following steps followed. For the DLC pure film, cleaning of the C targets and substrates was performed by applying a power of 1500 W on each C target and applying a bias voltage of 600 V on the substrates for 20 min. Then the Cr target was cleaned for 10 min applying a power of 2000W. For the DLC-Si and DLC-W films cleaning on the Cr and Si or C–W were conducted at the same time. In the Cr target a power of 2000 W was applied and on Si or C–W targets a power of 500W and 1200 W were applied. Independently of the system, then the carbon pure targets were cleaned applying the power as described for pure DLC coating. To improve the adhesion of the films, a Cr interlayer was deposited by applying 2000 W to the Cr target for 10 min and a pulsed negative bias of −110 V to the substrate support (deposition pressure of 0.37 Pa). A gradient layer of Cr was then deposited, by decreasing progressively the power applied to the Cr target for 10 min and turning on the C target. The final layer depositions followed with the parameters as summarized in Table 1, for the DLC, DLC-Si and DLC-W layers.

2.2. Characterisation of coatings

The elemental composition of the coatings was obtained with the use of X-ray wavelength dispersive spectroscopy (WDS) on a Zeiss Merlin SEM equipped with an Oxford Instruments WDS probe. The analysis was performed with 10 kV of acceleration tension, with a typical energy resolution of 3–30 eV, with an effective X-ray acquisition angle of 35° for the spectrometer. Six iterations were performed per sample. The images of the film's morphology were obtained in the same SEM device, however with 2 kV of acceleration of the electron beam. From the SEM images, the size of cauliflower-shaped top features in DLC coatings was

Table 1
Main deposition parameters.

Samples	Deposition pressure (Pa)	Ar flow (sccm)	Deposition time (min)	Power applied to targets (W)			
				C	Cr	W	Si
DLC-W	0.45	46	95	2x1750	0	1200	–
DLC	0.45	46	270	2x1750	0	–	–
DLC-Si	0.45	46	180	2x1750	0	–	500

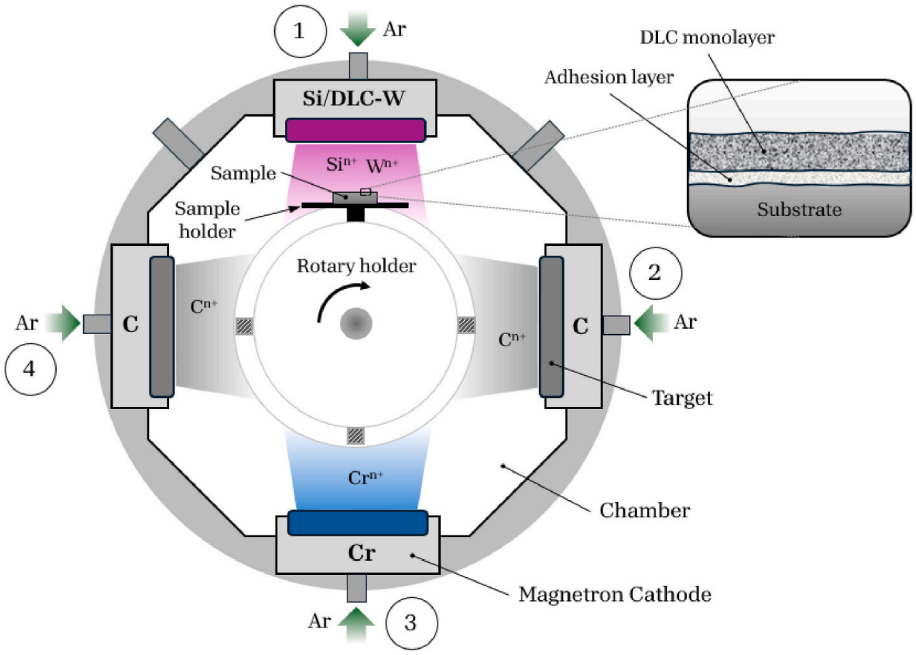

Fig. 1. Schematic illustration of the deposition chamber (magnetron sputtering) and distribution of the targets used for the deposited films.

measured using the standard linear intersection technique. To ensure representative results, three measurements in in four different areas were made.

The films were analysed by Raman spectroscopy to have information about the coatings structure. For that a confocal Raman spectrometer (Renishaw, In Via) was used, with a 532 nm laser and a 20× objective lens. All the measurements were performed with an exposure time of 30–50 s at 1 % power at room conditions. Three acquisitions were performed on three different areas of each sample. Raman spectra were deconvoluted using two symmetric Gaussian functions associated with the *D* and *G* peaks, with a linear background in the range 900–1800 cm^{-1}.

The hardness and reduced Young's modulus of the films were determined using a depth-sensing indentation technique (Micro Materials NanoTest platform). To avoid the influence of the substrate, a maximum load of 10 mN was applied, ensuring that the maximum indentation depth did not exceed 10 % of the total coating thickness [10].

2.3. Tribology tests

Alternative sliding friction tests were performed using a multifunctional tribometer (MFT-5000, RTEC Instruments) at ambient temperature of 25 °C ± 0.5 °C, in dry and lubricated conditions, and at 200 °C ± 0.5 °C, in dry conditions. A ball-on-plate configuration was used, according with ASTM G133 standard, with the parameters presented in Table 2. During the sliding tests, the dynamic coefficient of friction (*COF*) as a function of time was recorded. Three tests, for each condition, were performed, and the average specific wear rates were determined. A load of 10 N was applied to reach a maximum Hertzian pressure of 22.5 MPa. The lubricant used was CUT-MAX BR 500, a refined paraffinic mineral oil, with anti-corrosion and extreme pressure additives, suitable for severe metal machining.

Table 2
Parameters for reciprocating sliding test of sphere against coated samples.

Parameters	Values
Normal force	10 N
Frequency	7 Hz
Stroke length	8 mm
Test Duration	12 min
Total distance	160 m
Average velocity	4 mm/s
Counter-body	Inconel 718 (Φ ~10 mm)
Lubrication	Yes/no
Test environment condition	Unlubricated RT, Unlubricated 200 °C, Lubricated RT

After the tribological tests, the wear scars on the sliding partner were observed with an Alicona^{MT} Infinite Focus G5 microscope. The worn surfaces and debris were investigated using SEM-EDS and Raman spectroscopy to determine the dominant wear mechanisms. In addition, contact profilometry measurements were performed with a Taylor Hobson Form Talysurf 50L, equipped with a sensor tip radius *of* 2 μm diamond-tipped stylus with a resolution of less than 10 nm. The measurements were analysed with the educational version of Origin software to produce visual images and obtain depth and transverse wear data. Three measurements were acquired for each condition and the mean values were calculated. The area was multiplied by the track length to obtain the worn volumes. The specific wear rate, *k*, is calculated by dividing the worn volume *V* (mm^3) by the sliding distance (*mm*) and multiplying by the normal load *N* (*N*) Eq. (1) [30].

$$k = \frac{V}{N \cdot x} \quad \text{Eq. (1)}$$

To estimate the worn volume of the sliding counterpart (Inconel 718 sphere), the concept of 'apparent volume' was used (Fig. 2b). This estimate makes it possible to evaluate the contribution of the sphere to the total wear in the mutual interaction of the two bodies and to determine whether its wear is significant or negligible when it is minimal. The volume of a spherical section is calculated geometrically by Eq. (2). However, when scanning or capturing an image of the wear under microscopy, it is only possible to measure the worn area of the sphere. Therefore, this study proposes a way to estimate the worn volume "V_p" using Eq. (3), starting from Eq. (2) and determining a mean diameter "d" using Eq. (4).

$$V_p = \frac{\pi h^2}{3} \cdot (3R - h) \quad \text{Eq. (2)}$$

$$V_p = \frac{\pi}{3}\left(\frac{D}{2} - \sqrt{\frac{D^2}{4} - \frac{d^2}{4}}\right)^2 \left[3\frac{D}{2} - \left(\frac{D}{2} - \sqrt{\frac{D^2}{4} - \frac{d^2}{4}}\right)\right] \quad \text{Eq. (3)}$$

$$d = \frac{d_{max} + d_{min}}{2} \quad \text{Eq. (4)}$$

3. Results and discussion

3.1. Cross-sectional morphology and structure

Fig. 3 present the SEM cross-section morphologies of the as-deposited coatings. As expected, the DLC-based coatings present a columnar growth morphology. The AlTiSiN coating, presents a more compact morphology. Since the last coating was deposited in a *HiPIMS* power supply, the compact structure can be explained by the higher level of bombardment of the growing film and higher temperature used in the deposition [31].

The surface morphologies of the deposited films, obtained by SEM, are presented in Fig. 4. All DLC base coatings presents the typical cauliflower type surface morphology of *DCMS* sputtered coatings as observed in other works [10]. The surface morphologies are related with the cross-section morphology with the coatings with more compact columns showing smaller cauliflower morphology. The AlTiSiN coating presented a much more compact morphology that results in a more homogeneous surface morphology. Nonetheless, during the deposition process there are some instabilities, such as arching that might result in the formation of some defects on the coatings surface such as individual microdroplets [32].

The elemental chemical composition, thickness and deposition rate are presented in Table 3. The DLC-W and DLC-Si alloyed coatings present a similar alloying content near to 15 at. %. The lowest deposition rate was observed for pure DLC, since only two C targets were used to deposit the coating. The DLC-W and DLC-Si coatings have similar thicknesses; however, the deposition rate for the DLC-W is significantly higher as compared to other DLC base coatings due to the significant higher power applied on the target with the W pellets. The thickness of the coatings was set based on previous works [10,33].

Fig. 5 shows the surface topography of the DLC coatings obtained by 3D profilometry. The DLC coatings showed shallow protrusions with Sz values < 82 nm. Pure DLC and DLC-W presented the smoothest surfaces, with surface roughness (Sa) of 4.15 nm, 4.75 nm and maximum surface roughness height (Sz) of 42 nm and 45.7 nm, respectively (Fig. 5a and b), as compared to DLC-Si, whose surface roughness was Sa = 6.69 nm and Sz = 81.5 nm (Fig. 5c). Considering that in this study the bias voltage was kept constant in all the depositions, it appears that the main factor influencing the surface topography is the dopant elements [21]. This effect was observed in other studies such as that of Juan et al. [34]. However, for AlTiSiN film, the distribution of the surface perturbations (Fig. 5d), the Sz values are in average of 75 nm and maximum of approximately 150 nm. The higher Sz value of this film is attributed to the microdroplets found on their surface.

3.2. Raman analysis

Fig. 6a presents the Raman spectra of the deposited films, between 900 and 1800 cm^{-1} of the Raman shift. The two peaks named *D* and *G*, typical of DLC coatings, are observed at approximately 1350 and 1580 cm^{-1}, respectively. From the peak deconvolution three main parameters are obtained, the peak position, Full Width Half Maximum of the *G* peak (*G-FWHM*) and the *G* and *D* peaks intensity. Those parameters were used to determine the *ID/IG* ratio. The *G* peak is associated with vibrations of carbon atoms in a graphite structure (sp^2), while the *D* peak indicates the presence of defects or disorder in the structure (sp^2) [35].

The undoped DLC film shows a typical Raman spectra for this type of materials with the *G*-peak position at approx. 1568 cm^{-1} an *ID/IG* ratio of 1.19 and a *G-FWHM* of 286 cm^{-1}. The addition of an alloying element results in a variation of those parameters. Alloying with Si, results in a shift the *G*-peak position to 1514 cm^{-1}, while the *ID/IG* ratio decreases from 1.19 to 0.94. This shift of the G-peak and reduction of the *ID/IG* ratio are the result of changes of the type of bonding present and its clustering. This shift of the *G*-peak and the reduction of the *ID/IG* ratio led to changes in the microstructure of the undoped DLC films [36]. On the other hand, W doping increases the *ID/IG* ratio from 1.19 to 1.59 and the *FWHM* (full width at half maximum) from 286 to 353, without significantly affecting the relative position of the G peak at 1560 cm. This suggests an improvement in the quality of the coating, possibly due

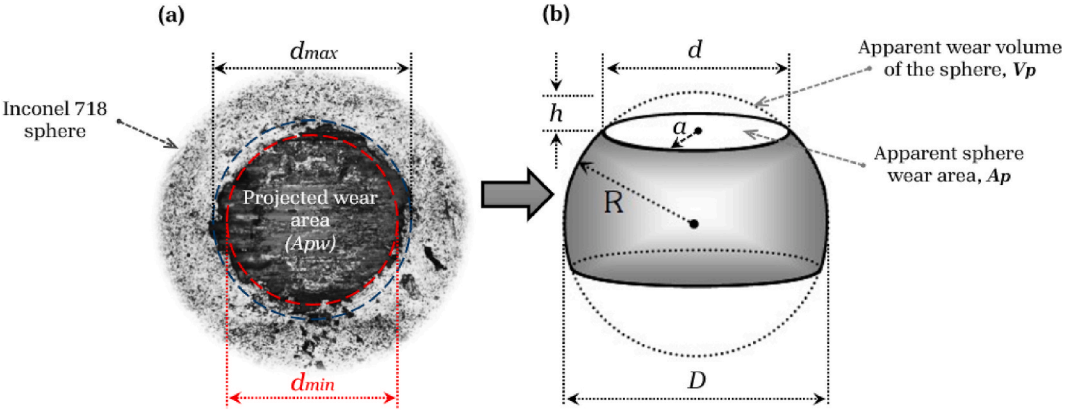

Fig. 2. Schematic representation for the determination of the wear volume in the Inconel 718 ball sphere. a) projected view of the wear zone with maximum and minimum diameters of the wear contour, and b) variables involved in determining the apparent wear volume.

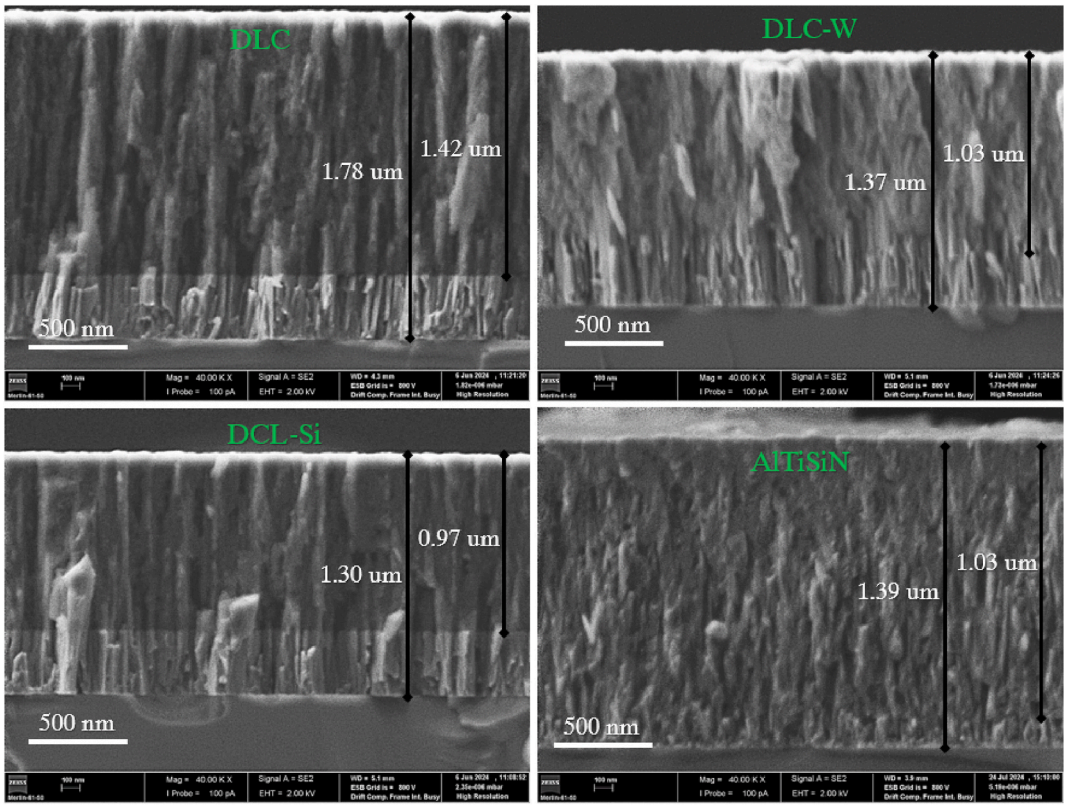

Fig. 3. Sectional structural morphology of the: pure DLC, DLC-W and DLC-Si and AlTiSiN coatings.

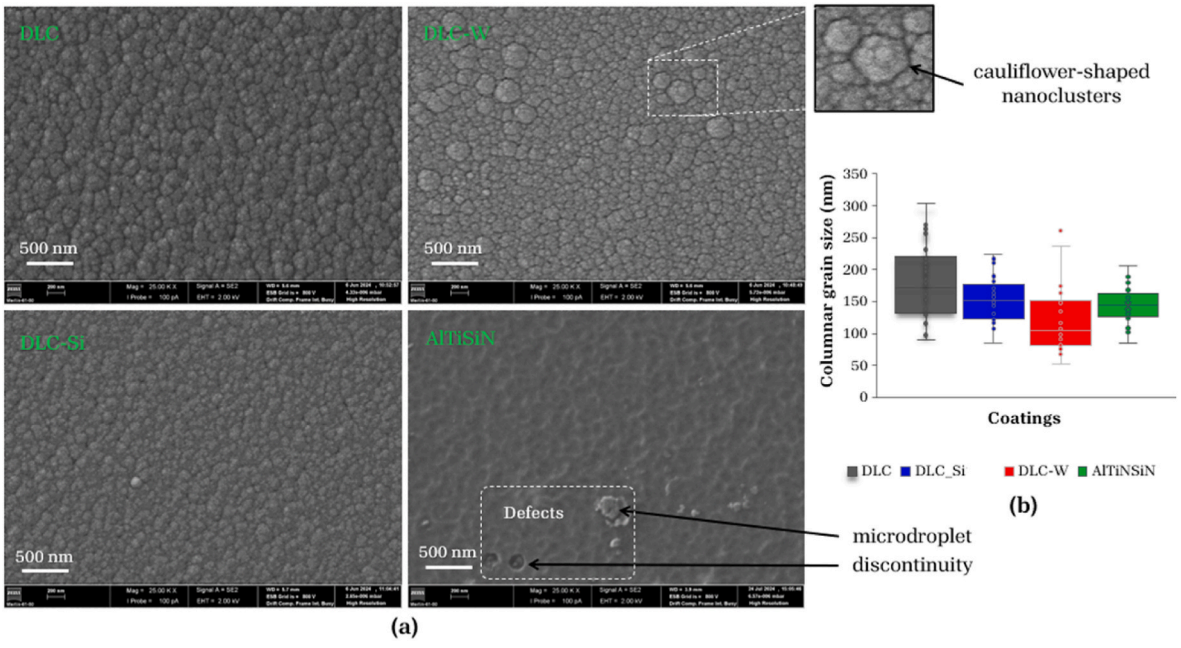

Fig. 4. SEM images of surface morphology of the deposited coatings (a). Size of cauliflower-shaped nanoclusters in DLC coatings (b).

to a higher disorder in the carbon structure, which may be related to a higher fraction of sp^3 bonds.

As for the Raman spectra of the AlTiSiN coating provided by the commercial company, it shows the common peaks characteristic of this film. The band around 258 cm^{-1} is associated with the vibrations of the Al–N and Ti–N bonds in the coating structure [37]. In contrast, the band around 600 cm^{-1} may be related to the vibrations of the Si–N bonds and possible combinations of vibrational modes in the structure [38].

3.3. Mechanical properties

The hardness - *H* and reduced Young's modulus - *Er* of the coatings were determined by nanoindentation with a maximum load of 10 mN and are shown in Fig. 7. The loading unloading curves are presented in

Table 3
Coatings chemical composition obtained by WDS, and depositions rate.

Coating	C (at. %)	O (at. %)	Cr (at. %)	Alloying (W, Si) (at. %)	Thickness (μm)	Deposition Rate (nm/min)
DLC_W	82.7	0.7	0.3	16.4	1.37	14.4
DLC	98.1	1.7	0.1	0.0	1.78	6.6
DLC_Si	84.6	0.5	0.2	14.7	1.30	7.2
	Al (at. %)	**Ti (at. %)**	**N (at. %)**	**Si (at. %)**		
AlTiSiN	3.3	55.2	61.6	4.2	1.69	19.9

Fig. 7a. The average reduced modulus (*Er*) of the three DLC coatings are similar, within the range of 170–190 GPa, while the Er for the AlTiSiN coating showed a significant higher value compared to the DLC films. The average hardness (*H*) of AlTiSiN is shown to be more than twice than that for the DLC coatings, resulting in the same increasing trend for the *H/Er* ratio (Fig. 7b).

Non-hydrogenated DLC coatings typically exhibit hardness values ranging from 10 to 20 GPa [16]. In the works of Hofmann [19], it was reported that incorporating 5 %–20 % Si into DLC coatings results in hardness (*H*) variations from 12 to 21 GPa. Similarly, Ferreira et al. [39] found that adjusting the bias voltage from floating to −100 V leads to hardness variations between 8 and 22 GPa. Previous studies, such as that of Evaristo et al. [33], reported hardness values of 16.1 ± 1.3 GPa for DLC-W and 17.7 ± 1.0 GPa for DLC-Si. Additionally, the reduced modulus (*Er*) was approximately 190 ± 1.3 GPa. Therefore, the hardness values obtained in this study for DLC coatings are comparable and consistent with those reported in the literature.

3.4. Frictional behaviour

The evolution of the coefficient of friction (*COF*) for all coatings, under the different test conditions, are presented in Fig. 8. In dry conditions, the DLC coating shows an instability in the first 25 m of sliding and then stabilizes. The test of the pure DLC film starts with a slight oscillation of the *COF* that normally are associated with the accommodation of the surfaces in contact (running in stage). Then, in the first 15 m there is a gradually decrease the *COF* from 0.2 to 0.15 until 25 m of sliding, that could be associated with the formation of the tribolayer with self-lubricant characteristics. After reaching 25 m, the *COF* remains constant until the end of the test. The *COF* for the test at RT in dry conditions for the DLC-W film decreases faster than pure DLC to 0.15 at a sliding distance of 2 m of sliding and then increases slightly to 0.17 at 25 m of sliding distance and stabilizes at this value until the end of the test. The DLC-Si film showed the lowest *COF* reaching 0.09 at 4 m of sliding and then gradually increases with some oscillations and until 30 m and then stabilizing with lowest *COF* of all coatings. On the other hand, the AlTiSiN film showed a *COF* 3 times higher and with high instability compared to the DLC coatings, remaining between values of 0.68 and 0.73 showing that this coating does not have self-lubricant characteristics.

At 200 °C (Fig. 8b), all DLC-based coatings (DLC and DLC-Si) exhibited an increase in friction compared to the room temperature (RT) tests. The increased friction is attributed to the removal of moisture from the sliding contacts as the sample is heated to 200 °C, as it is well known that moisture plays a crucial role in reducing friction for non-hydrogenated DLC coatings. The coefficient of friction (*COF*) of the DLC-W coating at 200 °C is not reported due to premature failure of the coating during the test. The DLC-Si coating displayed an increase in *COF* from 0.33 to 0.45 after the running-in stage. On the other hand, the pure DLC film displayed the lowest *COF* under these conditions with a value of 0.15 that was maintained up to a sliding distance of 415 m. The AlTiSiN film, shows a stable *COF* throughout the test, maintaining a value of 0.62, demonstrating a certain stability with temperature changes during sliding.

When the test was performed under lubricated conditions at room temperature, three different behaviours were observed. The DLC-W coating displayed the highest *COF* with a gradual decrease of the friction during the sliding test with some instabilities of the *COF* during the

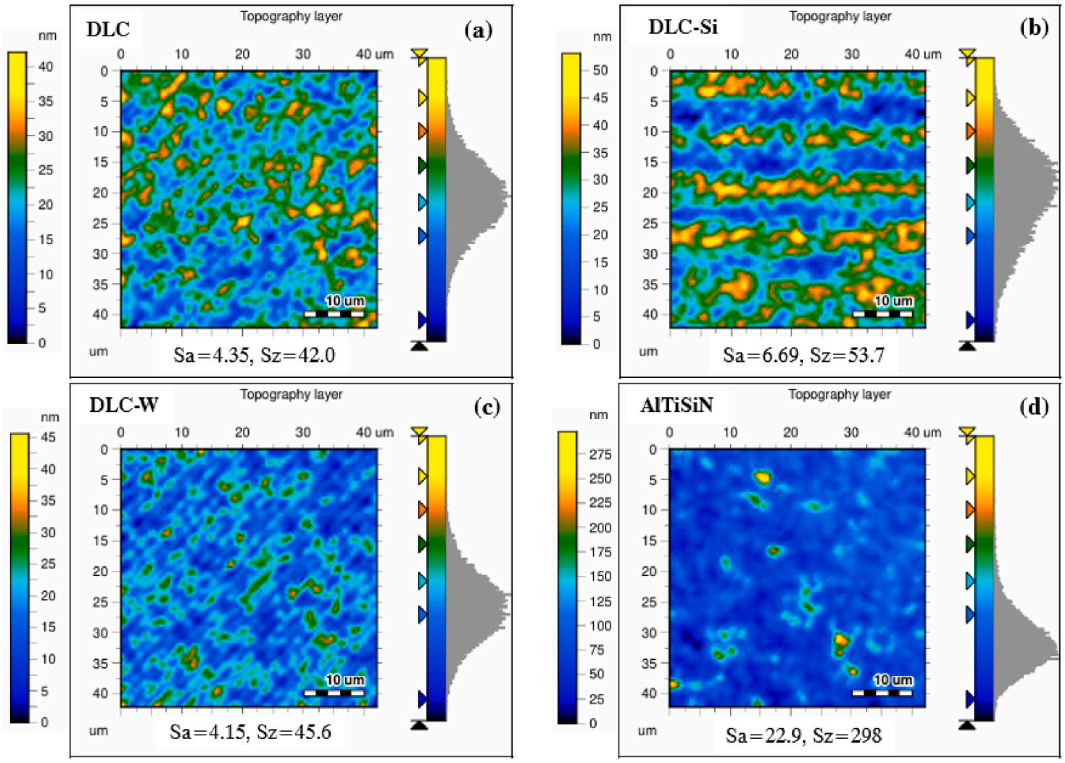

Fig. 5. Surface topography Sa of deposited coatings: (a) DLC, (b) DLC_Si10 %, (c) DLC_W, and (d) AlTiSiN.

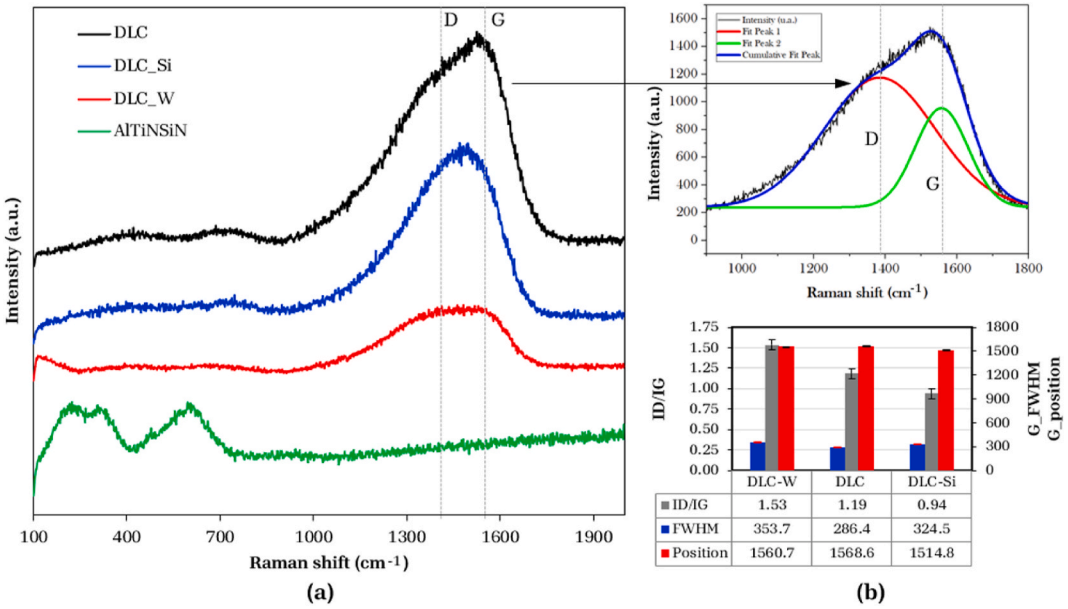

Fig. 6. Raman peaks, a) deposited films, and b) signal convolution and intensity ratios of DLC films.

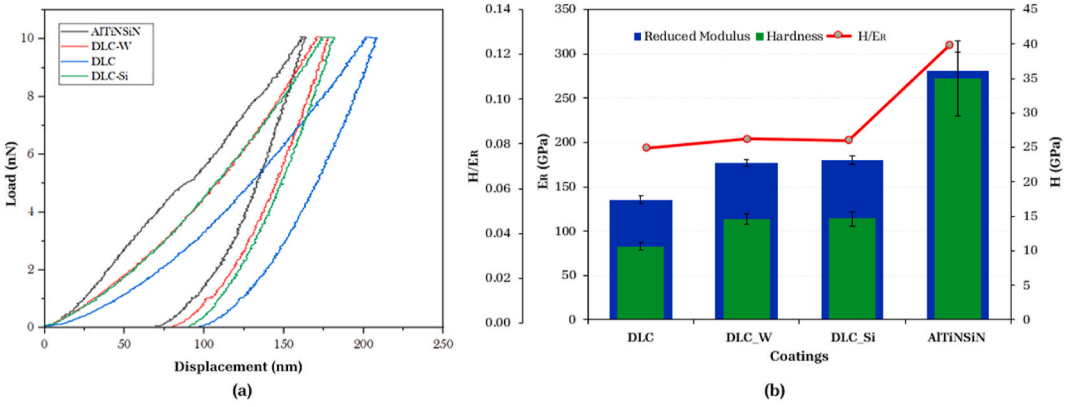

Fig. 7. Mechanical properties of the coatings measured by nanoindentation with a maximum load of 10 mN. a) Average load unloading versus displacement curves, b) Hardness (*H*), Reduced Modulus (*Er*), and Mean *H/Er* ratio.

test. The DLC and the DLC-Si presented remarkably similar *COF* with a gradual decrease of the friction during the test reaching a value lower than 0.05. The AlTiSiN coating presented a friction coefficient in between the other coatings, which was stable throughout the whole test.

3.5. Specific wear rate of coatings

Fig. 9 shows the results of the wear performance of the coatings and its sliding partners. The wear rate of the coatings measured from the "sliding wear track (*Swt*)", for the different test conditions are presented in Fig. 9a. The wear rate of the balls was calculated, by the "Projected wear area (*Apw*)" and the results are presented in Fig. 9b.

The specific wear rate of the coatings varies significantly under different testing conditions, including dry, room temperature (RT), and 200 °C. *Swt* graph reveals that under dry conditions, all coatings experience higher wear due to increased friction and the absence of a lubricating layer to minimize direct contact between surfaces. At room temperature, DLC exhibits moderate wear resistance, but its wear rate rises sharply at 200 °C, which can be attributed to graphitization-induced structural degradation. The silicon-doped - DLC_Si) demonstrates lower *Swt* as compared to pure DLC under all conditions, indicating that silicon enhances thermal stability and wear resistance. The tungsten-doped -DLC_W coating did not outperform the undoped DLC coating tested at dry room temperature conditions. However, under lubricated conditions, it exhibited the lowest specific wear rate, although it did not surpass the performance of AlTiSiN. Generally, tungsten-doped DLC is known for its hardness and thermal stability, which enhances its resistance to sliding wear. Nevertheless, in this test, it showed lower resistance against Inconel 718, possibly due to inadequate adhesion The AlTiSiN coating consistently shows the lowest specific wear rate in all conditions, particularly at 200 °C, reinforcing its superior thermal stability and resistance to oxidative and adhesive wear. The projected wear area (*Apw*) on the Inconel ball confirms the wear trends observed on the sliding tracks of the DLC coatings. At room temperature (RT), the *Apw* values are similar for the DLC coatings, with the lowest wear on pure DLC, followed by DLC-Si and finally DLC-W. In contrast, the *Apw* in the case of sliding on AlTiSiN showed the highest value among all conditions evaluated, indicating a higher wear of the Inconel sphere, evidenced by a larger footprint. Fig. 10 presents the profile of the footprint for the different tests. The width of the profile is proportional to the *Apw* on the Inconel sphere, which is logical: the wider the footprint, the greater the wear on the sphere. However, the profiles also reveal that the smaller footprint depth in the AlTiSiN coating is due to its high wear resistance, which results in a lower wear

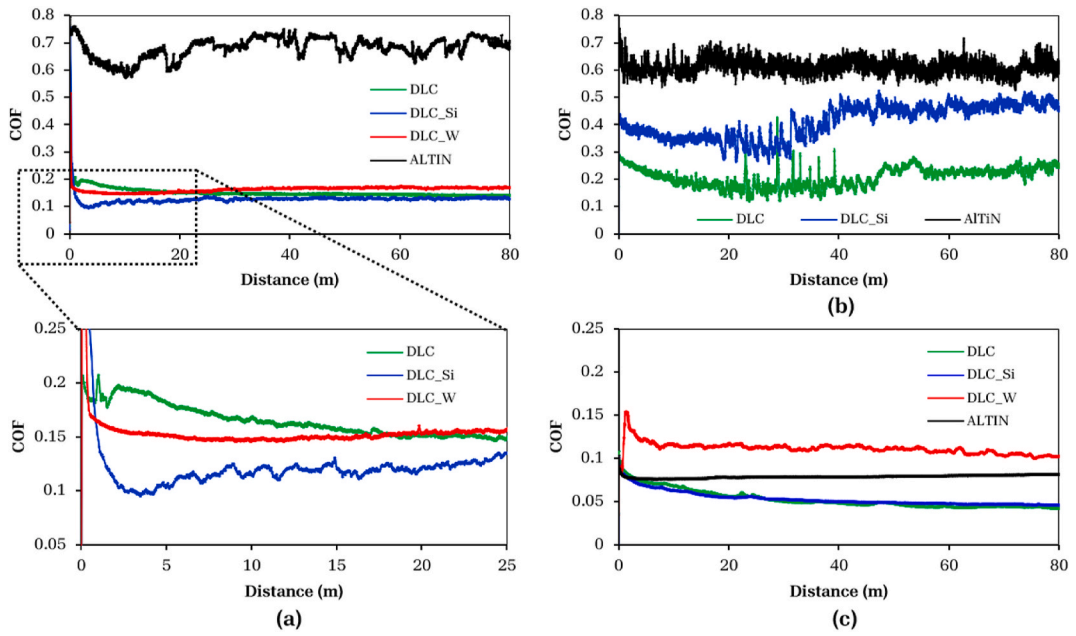

Fig. 8. Evolution of the coefficient of friction (*COF*) of the coatings as a function of total sliding distance, under the following conditions: a) dry at room temperature, b) dry at 200 °C, and c) lubricated at room temperature, with a load of 10 N, a frequency of 7 Hz, and a distance 160 m a counter-body of Inconel 718.

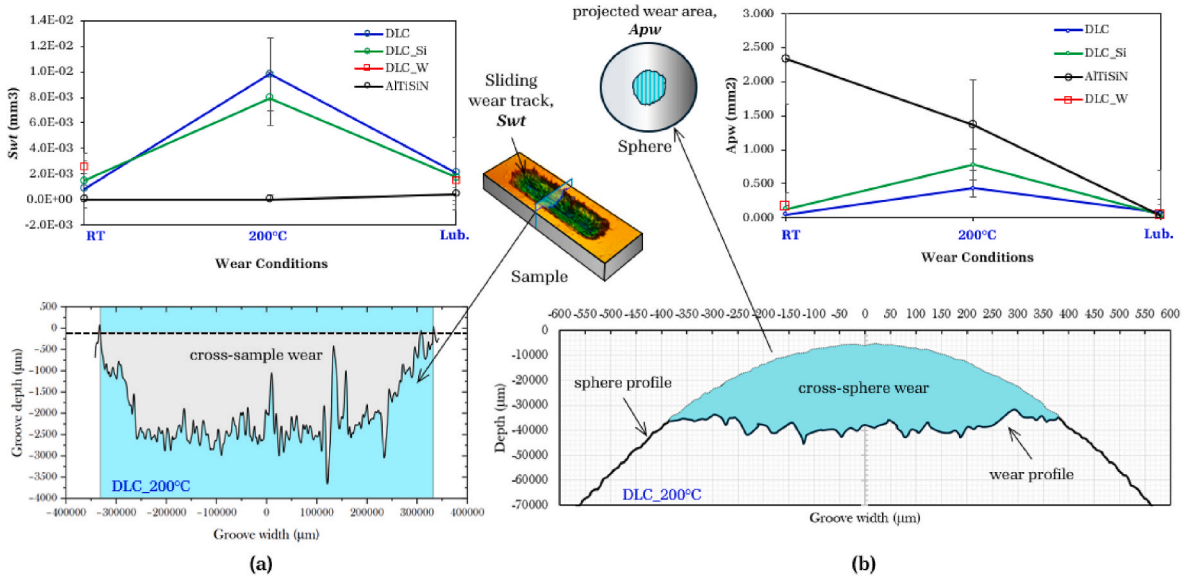

Fig. 9. Results of wear indicators and profilometry of the reciprocating sliding test of an Inconel sphere against deposited coatings with a load of 10 N, frequency of 7 Hz and distance of 160 m: (a) Sample, (b) Sphere.

rate, as shown in Fig. 9a. The higher specific wear rate of the counterpart on the tests conducted against the AlTiSiN coating is caused by the much higher hardness of this coating as compared to DLC coatings and due to the high friction generated.

At 200 °C, the transverse wear profiles of the DLC coatings show wider and deeper tracks, which is evidence of higher material loss due to thermal softening and adhesive wear mechanisms. The only exception is the AlTiSiN coating, whose profile and *Apw* are lower. In dry and high temperature conditions, the interaction between surfaces intensifies, increasing friction and wear. These results agree with the literature, which points out the limitations of DLC at high temperatures and the benefits of dopants such as silicon and tungsten. Furthermore, the exceptional wear resistance of AlTiSiN under all conditions confirms its suitability for applications requiring high durability in dry and high temperature environments, such as cutting tools and tribological components.

Under lubricated sliding conditions, the *Apw* remains low and similar for all coatings. However, this effect is particularly beneficial in the case of AlTiSiN, as it reduces the *Apw* and minimises the loss of coating material. This indicates that the lubricant decreases the contact and friction between the Inconel sphere and the coating. In contrast, for the DLC coatings, the lubricant does not have a significant impact, as the *Apw* retains similar values to those observed at RT conditions, with only a minimal reduction.

Finally, Fig. 11 shows the specific wear rate (k) of the coatings in the different experimental conditions, both for the coatings (Fig. 11a) and for the Inconel ball (Fig. 11b). The trends observed are consistent with the volume and area wear results previously shown in Fig. 9a and b

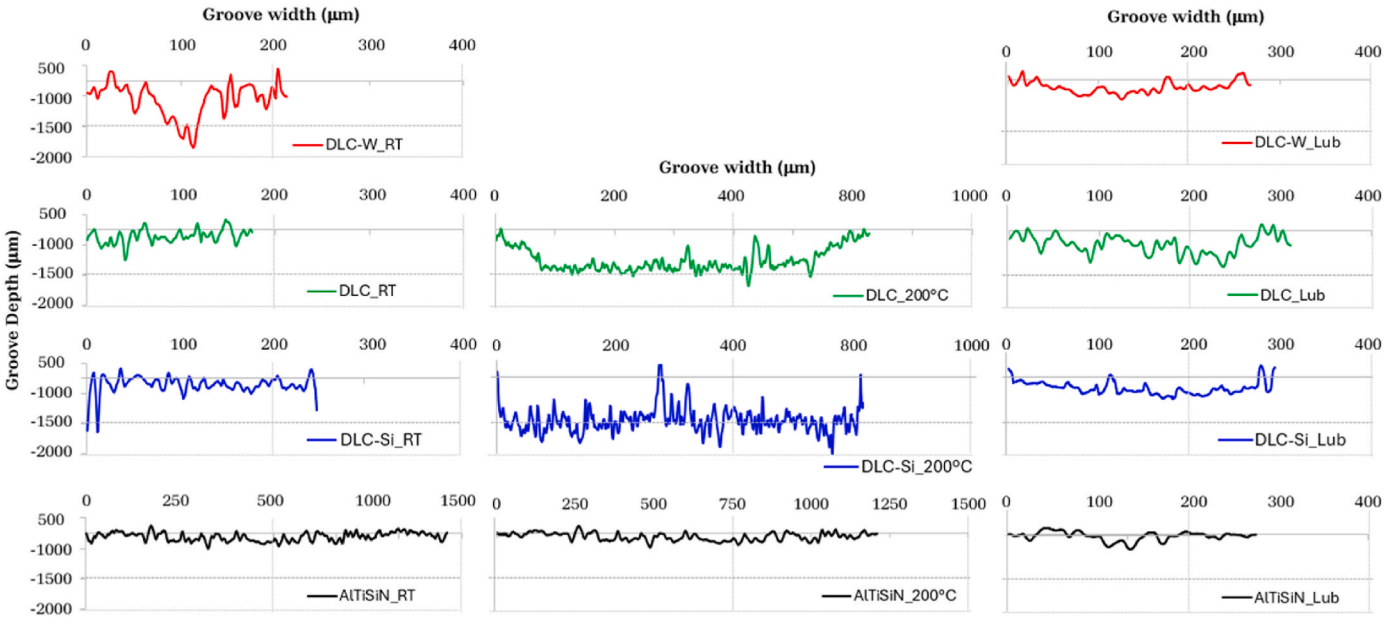

Fig. 10. 2D wear profiles extracted from the 3D topography of the wear tracks of DLC and AlTiSiN coatings tested at different sliding conditions.

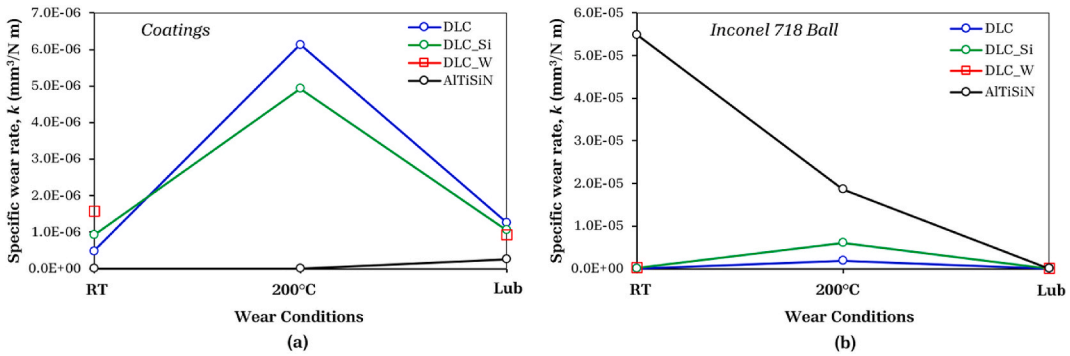

Fig. 11. Specific wear rate results for the coatings under the different experimental conditions, a) coatings and b) Inconel 718 ball.

because of their direct relationship. However, these values also show the aggressiveness of Inconel for coating wear, as the study by Jiang [40] reports lower specific wear rates even when the load is increased to 20 N and 40 N, or despite similar or higher surface roughness (Ra). In this study, the average substrate roughness is Ra = 0.05 µm. It is likely that the higher value of k is due to the combination of the short reciprocating distance (8 mm) and the frequency used (7 Hz), which creates a concentration of heat in the contact zone. This effect is particularly detrimental to DLC coatings.

3.6. Surface analysis of worn areas

The surface analysis of the worn areas provides crucial insights into the wear mechanisms governing each coating under different testing conditions, including dry, room temperature (RT), and elevated temperatures of 200 °C. The worn surfaces of DLC coatings reveal distinct wear characteristics depending on the testing environment. Under dry conditions, DLC exhibits abrasive wear features, with ploughing marks and micro-fractures indicating material removal due to the absence of lubrication (Fig. 12). At room temperature, DLC shows relatively smoother worn surfaces but still displays signs of adhesive wear, suggesting localized material transfer between the coating and counterbody. However, at 200 °C, the wear surface becomes rougher with evidence of severe material degradation, consistent with graphitization, which reduces the coating's mechanical strength and accelerates wear. The DLC_Si coating demonstrates a more stable wear surface with reduced micro-cracks and wear debris, indicating improved thermal resistance and lower material loss compared to undoped DLC. This aligns with the lower specific wear rate and projected wear area (*Apw*) observed for DLC_Si, reinforcing the beneficial role of silicon in enhancing wear resistance.

Under room temperature (RT) conditions, tungsten-doped DLC (DLC_W) exhibits more pronounced wear than pure DLC, with more severe surface damage. Worn surfaces show increased adhesive patchiness, intense plastic deformation and micro-cracks, suggesting premature coating failure due to severe dry contact. In addition, the formation of nickel and chromium oxides from Inconel 718 could intensify abrasive and adhesive wear, as observed on the surface of the sphere. However, under lubricated conditions, the wear rate of DLC_W is lower than that of DLC-Si and pure DLC, which prevents concluding a low overall performance. Under these conditions, its wear rate is like that of AlTiSiN, although the latter shows less surface damage in all tests, with minimal wear scars and shallow imprints, even at 200 °C.

The worn surface of AlTiSiN remains relatively smooth, with only slight polishing effects observed, confirming its superior resistance to adhesive and abrasive wear. Transverse wear profiles (Fig. 10) further corroborate these results, revealing that the depth of wear tracks is significantly greater for DLC at 200 °C compared to RT, highlighting the

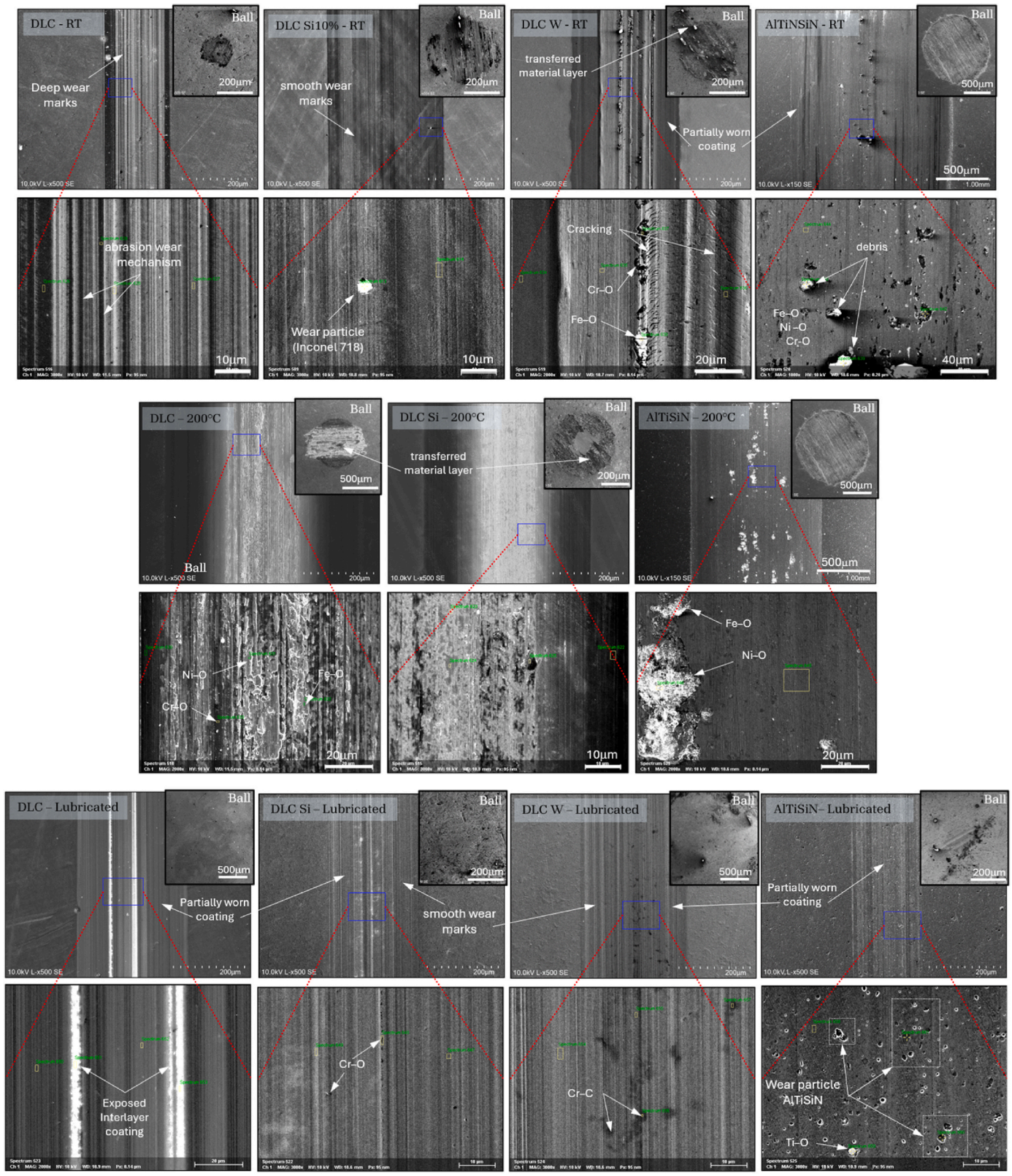

Fig. 12. Surface wear analysis of samples after RT room temperature reciprocating sliding test of an Inconel sphere against coatings deposited with a load of 10 N, a frequency of 7 Hz and 160 m.

role of thermal degradation in increasing material loss. In contrast, DLC_Si shows shallower wear tracks, demonstrating its higher wear resistance under high temperature conditions. AlTiSiN, on the other hand, maintains the lowest wear depth at all conditions, confirming its exceptional thermal stability. The counter-body interaction is also evident in the cross-sphere wear profiles, where higher material transfer and surface roughness is observed at 200 °C for the DLC coatings, while AlTiSiN shows minimal counter-body wear, reducing overall friction

and wear rates. These observations are consistent with existing literature, which highlights the thermal limitations of DLC coatings and the advantages of doping elements such as silicon to improve wear resistance at high temperatures. The findings further validate the superior performance of AlTiSiN, making it the most suitable coating for applications involving extreme temperatures and high loads, such as cutting tools and tribological components.

The EDS results of the wear track under RT conditions show no significant difference from the pristine surface composition, meaning that the wear of the coatings was very superficial. However, in the DLC_W track, which experienced the most significant amount of wear, and the wear profile demonstrates this. On the worn surface there is evidence of iron oxide particles adhering to the entire track, where the DLC film had degraded substantially and had almost lost its full thickness. The wear track of the AlTiSiN coating was characterised by debris corresponding to common oxides resulting from the wear of the Inconel sphere. As illustrated in Fig. 9a, the temperature of 200 °C resulted in an increase of the wear rate for all DLC coatings, with the DLC-Si coating presenting the lowest value. Raman spectroscopy of the abraded surfaces showed in Fig. 13, for the DLC coating an increase in the intensity of peaks *D* and *G*, accompanied by slight shift to higher frequencies and broader full width at half-maximum (*FWHM*) values, for peak *D*. This suggests that the heating process influenced the structural integrity of the coatings. Pure DLC showed signs of graphitization, reflected in the changes in peaks *G* and *D*. In contrast, DLC-Si showed better thermal stability since only small variations on *ID/IG* were observed, while DLC-W experienced accelerated graphitization potentially attributable to the presence of W.

As predicted, the interaction between the coatings and Inconel 718 in lubricated conditions created a favourable tribological environment, which significantly reduced friction-induced wear, particularly adhesive wear. Only residual AlTiSiN coating particles resulting from abrasion were observed. Raman analysis revealed that mineral oil mitigated the severity of structural changes in the DLC coatings, although it did not completely eliminate surface graphitization, especially for DLC-W. Notably, DLC-Si exhibited the highest resistance to structural changes due to silicon's stabilizing effect, whereas pure DLC and DLC-W were more susceptible to structural transformation, as reflected in the Raman spectrum by more intense and shifted peaks (Fig. 13a). This effect is evident in the changes of the ID/IG ratio for each condition tested (Fig. 13b).

The evidence of adhesive wear suffered by the Inconel sphere is shown in Fig. 14. The compositions of the transfer layers evaluated at different points on the Inconel spheres were similar for all the DLC films. They show the presence of free C, and doping elements of each coating (Si–C, W–C, Si–O, W–O). As expected, the presence of free C is higher in the Inconel sphere, as evidenced by black zones on the surface (Fig. 14, lower left image). Likewise, the chemical composition of the wear debris scattered around the corresponding wear tracks suggests the presence of Fe–O and Cr–O.

EDS analysis on the abraded surface of the Inconel sphere reveals the presence of carbon layers (Table 4). In the wear zone that slide against pure DLC, free carbon residues were observed. The presence of carbon on the surface that slide against DLC-Si was also detected. The presence of dopant elements is observed on the abraded surface of the sphere in the form of particle that most probably are Si oxides in the case of sliding against DLC-Si10 %. For the DLC-W similar behaviour was observed with the presence of W on the transfer layer on the ball with the presence of O suggesting the formation of oxides. On particles e other hand, upon friction with AlTiSiN, the presence of Al and Ti residues adhered on the entire worn surface of the Inconel sphere was evidenced. This reflects the higher friction observed of this coating. High amounts of C are also detected in surface of the counterpart. However, contrary to the test conducted against the DLC coatings the C does not come from the coating. In fact, this coating is C free and therefore his concentration can only come from contamination due to specimens handling.

When the test temperature was increased to 200 °C, the transfer layer formed on the worn Inconel surface increased significantly upon test with the DLC coating (Fig. 15). The carbon-rich transfer layer is evident in the EDS spectra obtained at different zone of the sliding surface. This suggests an increase in the adhesive wear mechanism on the sphere since it was also observed am increase of the friction. In contrast, when sliding occurs against AlTiSiN, there is a reduction in wear (Fig. 9b), accompanied by an increase in oxidation. The growth of oxide layers may have responsible for the reduction in the coefficient of friction, which could have mitigated the aggressive wear experienced under room temperature conditions.

On worn ball surfaces the material transfer is minimal. The surfaces are relatively clean, and the dominant abrasive wear mechanism is observed. The EDS analysis detects carbon residues as well as the presence of S, Ca, Cl, K, Mg. The percentage of oxygen does not differ, so the presence of sulphur oxides is minor, accompanied by possible sulphates and chlorates due to the reaction with the mineral lubricating oil.

3.7. Discussion

The tribological interaction between DLC, DLC-Si, DLC-W, and AlTiSiN coatings with an Inconel 718 sphere under ambient temperature (RT), 200 °C, and mineral oil lubrication conditions shows differentiated behaviours in terms of wear and friction (*COF*). AlTiSiN presented the lowest wear rate with similar values for the three conditions tested due to its high hardness, approximately twice of DLC. However, this high

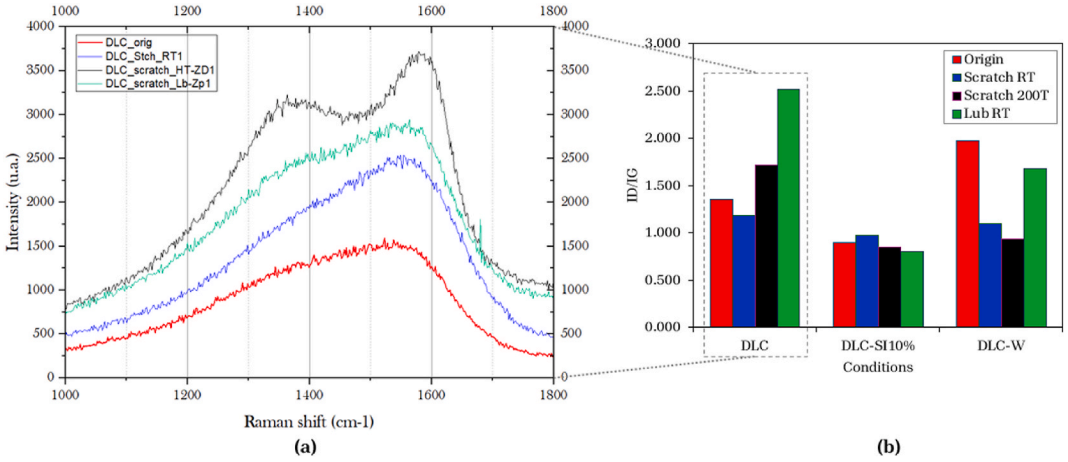

Fig. 13. Raman peaks, a) Spectra on abraded DLC coating surfaces at all sliding conditions, and b) intensity of ID/IG ratios of DLC films at all sliding conditions.

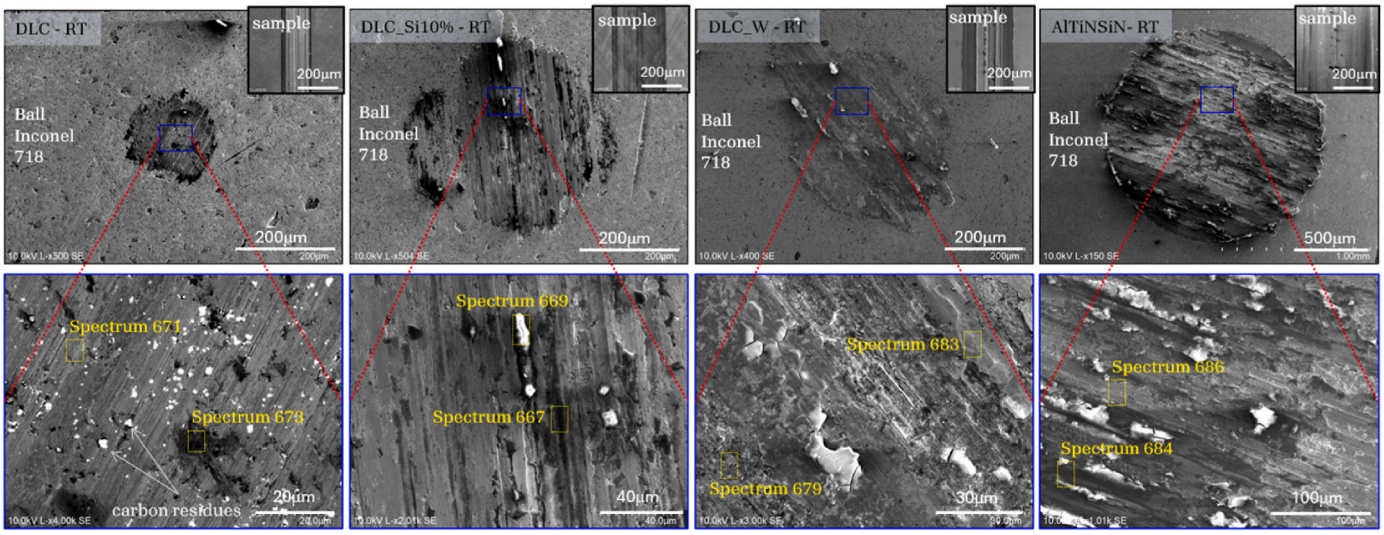

Fig. 14. Surface wear analysis of Inconel 718 spheres after room temperature reciprocating sliding test against coatings deposited with a load of 10 N, a frequency of 7 Hz, and 160 m.

Table 4
Result of EDS analysis on worn areas of Inconel 718 spheres after reciprocating sliding against coatings under RT conditions. The analysed spectra are over the locations shown in Fig. 11.

Spectrum	C	N	O	Si	Al	Ar	Ti	Cr	Fe	Ni	Nb	W	Mo
671	11.36	–	10.43	–	1.48	–	1.01	17.63	17.07	37.29	2.19	–	1.52
673	47.36	–	35.98	–	0.27	–	–	3.79	5.46	6.37	0.40	–	0.37
667	51.34	–	33.94	6.69	–	–	–	1.86	1.78	4.03	0.22	–	0.14
669	23.41	–	55.46	17.62	–	–	–	1.23	–	–	–	–	–
679	38.95	–	19.15	–	–	0.49	0.35	5.97	22.80	8.23	0.41	3.38	0.27
683	12.83	–	65.99	–	–	–	–	2.26	6.12	1.25	–	11.55	–
684	6.06	–	66.07	–	0.43	–	1.15	5.53	6.69	12.49	0.77	–	0.50
686	12.24	–	6.29	–	0.91	–	1.01	17.60	19.78	38.54	2.21	–	1.41

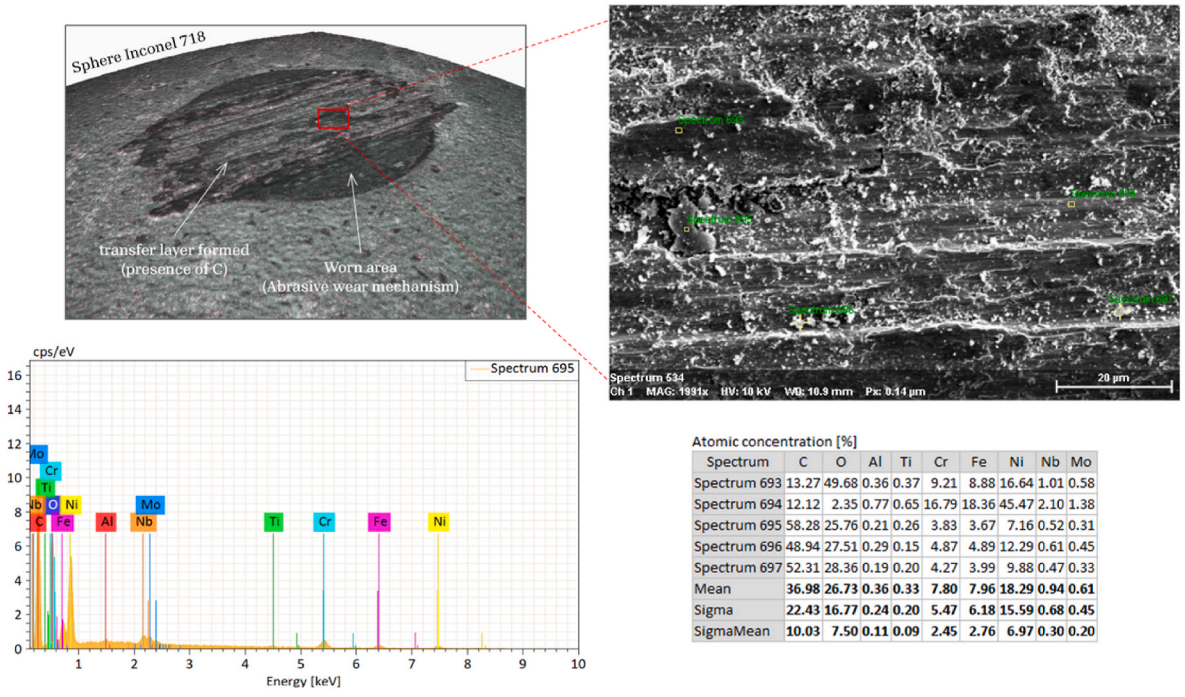

Fig. 15. EDS analysis of the transfer layer formed on the abraded surface of Inconel 718 sphere sliding on DLC coating at 200 °C.

hardness caused higher wear in the Inconel counterpart, showing its significant abrasive and adhesive wear. Suppliers of state-of-the-art AlTiSiN coatings [41] claim that they can withstand service temperatures up to 1100 °C, demonstrating their stability by retaining their hardness and toughness under extreme service conditions. On the other hand, DLC coatings experienced a considerable increase in wear rate at 200 °C, being 3 to 4 times higher compared to RT, reflecting a higher susceptibility to thermal degradation, by sp^3 to sp^2 bond transformation and surface oxidation, evidenced in Raman and EDS analysis respectively. Despite this, among the DLC coatings, the Si doped one was more resistant to wear at 200 °C because its presence stabilizes the sp^3 bonds when the temperature increases [42]. Likewise, the Si–O phase in the contact benefited the friction attenuation which allowed to have the lowest *COF* at RT as previous works have shown [43].

At room temperature, DLC-W, DLC and DLC-Si coatings exhibited lower coefficients of friction (0.16, 0.14 and 0.12, respectively), indicating good tribological performance and less interaction with the Inconel surface. However, as the temperature was raised to 200 °C, the *COFs* increased, indicating a partial decrease in the stability of the protective layer. With the increase of the temperature to 200 °C all the moister is removed from the sliding surfaces and it is known for non-hydrogenated DLC coatings the moister contributes for the low friction performance. In contrast, AlTiSiN had a high *COF* at room temperature (0.68), with a slight decrease to 0.60 at 200 °C, showing significant debris and oxidation, yet demonstrated wear stability in all three conditions tested. According to the literature, aluminum titanium nitride (AlTiN) offers high oxidation resistance compared to DLC-based coatings [12,37], which explains its wide application in high-performance cutting tools. Several studies have pointed out that AlTiSiN represents an evolution of AlTiN, due to the incorporation of silicon in its composition [32,44,45]. This element significantly improves the thermal stability of the coating by promoting the formation of an amorphous and dense silicon nitride phase, which acts as a barrier against element diffusion [32]. As a result, AlTiSiN has demonstrated superior performance in applications involving high speeds and friction at elevated temperatures, such as machining [44,45]. Its excellent sliding behaviour against Inconel 718 reinforces its suitability for demanding environments where wear resistance and thermal stability are critical factors.

Looking at the AltiSiN film in particular, its achieved hardness of 35 GPa confirms its excellent wear resistance and its ability to withstand plastic deformation [46]. This value, within the typical range of 30–35 GPa [47], makes it ideal for components exposed to severe sliding conditions. However, its reduced modulus (*Er*) of 180 GPa is significantly lower than the usual range of 350–400 GPa, suggesting a lower elastic stiffness. As for its *H/Er* value of 0.125, it represents a reasonable balance between toughness and elasticity. While it does not reach the upper limit of crack resistance (usual *H/Er* is between 0.1 and 1.20 [48]), it would still be suitable for applications with moderate loads or controlled impacts. The coefficient of friction (*COF*) of 0.68 at room temperature is slightly above the typical range (0.4–0.6), indicating higher initial friction. However, its reduction to 0.61 at 200 °C suggests better tribological performance at elevated temperatures, probably due to the formation of protective oxide layers. On the other hand, The Raman spectrum of the AlTiSiN coating reveals distinct peaks at 230, 290 and 600 cm^{-1}, providing valuable information about its amorphous structure. The peak at 230 cm^{-1} is probably associated with vibrational modes of metallic bonds, such as Ti–N or Al–N, which are commonly found in coatings based on metal nitrides [37,38]. This suggests the presence of an amorphous network dominated by metal bonds. The 290 cm^{-1} peak may correspond to vibrational interactions between aluminium and titanium atoms within the amorphous matrix, which could indicate the existence of disordered phases or interactions between the various components of the coating. The 600 cm^{-1} peak, associated with high energy vibrations, is probably linked to strong Si–N bonds, implying that silicon contributes to the structural rigidity and complexity of the amorphous network [49]. In addition, a characteristic peak near 480 cm^{-1}, commonly associated with amorphous silicon [49,50], was also detected in this study, confirming the presence of disordered Si bonds. Taken together, these spectral features suggest that the AlTiSiN coating possesses a mixed amorphous structure with both metallic and covalent bonds, which may influence the improvement of its mechanical and thermal properties as reported in the literature [41,45,47].

Under lubricated conditions, DLCs and their doped variants demonstrated a notable reduction in *COF* (0.052 for DLC and 0.053 for DLC-Si), confirming the self-lubricating effectiveness of these coatings in the presence of mineral oil, with minimal changes in structure detected by Raman spectroscopy. However, no clear reduction of the wear rate was observed, which remained at levels like those observed under dry conditions, indicating that the inherent self-lubricating effect of DLCs is highly efficient even without external lubrication. In contrast, AlTiSiN showed a moderate *COF* of 0.079 under lubrication, but its wear remained constant, highlighting its exceptional wear resistance even compared to DLCs, at the cost of higher aggressiveness towards Inconel due to its hardness.

4. Conclusion

In this work, the tribological behaviour of DLC coatings with different doping elements and AlTiSiN when sliding against Inconel 718 spheres has been experimentally investigated and compared, and the following conclusions have been drawn.

- The AlTiSiN coating presented the highest coefficient of friction (*COF*) among the coatings studied, showed the lowest wear rate in all conditions tested (RT, 200 °C and under lubrication). This is attributed to its high hardness, approximately twice that of the DLC coatings, which provides excellent wear resistance even at elevated temperatures and under lubrication. This high hardness also resulted in significantly higher wear of the Inconel 718 counterpart, suggesting a more aggressive abrasive and adhesive mechanism in the tribological interaction.
- DLC, DLC-Si, and DLC-W coatings demonstrated excellent self-lubricating behaviour with low *COFs* (0.14–0.16), especially in lubricated conditions (0.052–0.11), although with identical wear rates was observed in dry conditions. This suggests that the self-lubricating capability of DLCs is sufficient to maintain low friction with the lack of lubricant, which may be advantageous in applications where the use of lubricant must be avoid.
- DLC coatings and their doped variants showed a significant increase in wear rate when subjected to 200 °C, with values 3 to 4 times higher than at room temperature conditions, indicating increased susceptibility to thermal degradation. Raman analyses indicated that the graphitization of the sliding surfaces with the formation of oxides of the doping elements are the main wear mechanisms, especially in DLC-W.
- Despite the aggressive nature of sliding against Inconel 718, DLC and AlTiSiN coatings demonstrated specific benefits: DLC significantly reduced the coefficient of friction, while AlTiSiN showed improved wear resistance. Therefore, AlTiSiN is emerging as a promising option for coatings on cutting tools intended for machining Inconel 718. In contrast, DLC coatings may be suitable for low-speed applications and temperatures below 300 °C. Future studies will address the performance of these coatings under real mechanical conditions.

Author contributions

Conceptualization: Filipe Fernandes, Cristian Pérez-Salinas; Methodology: Filipe Fernandes; Preparations and Tests: Manuel Evaristo, Cristian Pérez-Salinas; Formal analysis and investigation: Cristian Pérez-Salinas, Manuel Evaristo; Writing - original draft preparation: Cristian

Pérez-Salinas; Writing - review and editing: Manuel Evaristo, Filipe Fernandes; Funding acquisition: Albano Cavaleiro; Resources: Albano Cavaleiro; Supervision: Norberto de Lacalle, Filipe Fernandes.

Declaration of generative AI and AI-assisted technologies in the writing process

During the preparation of this paper, the authors used [The ChatGPT Tool] in order to [improve writing and translation into English]. After using this tool/service, the author(s) reviewed and edited the content as necessary and take full responsibility for the content of the published article.

Declaration of competing interest

The authors declare that they have no known competing financial interests or personal relationships that could have appeared to influence the work reported in this paper.

Acknowledgements

Filipe Fernandes acknowledge the national funds through FCT – Fundação para a Ciência e a Tecnologia, under projects UID/00285 - Centre for Mechanical Engineering, Materials and Processes and LA/P/0112/2020.

The authors are thankful to project NEOPHYM, ref PID2022–137380OB-I00, funded by MCIN/AEI/10.13039/501100011033 and to the grant provided by Basque Government IT1573-22. Data monitoring was developed using the initial developments of Transmisiones SARA so thanks are due to PLEC2024-011247 funded by MICIU/AEI/10.13039/501100011033 and FEDER, UE.

Special thanks to the Universidad Técnica de Ambato for their collaboration and research support financed by resolution 0371-CU-P-2021.

References

[1] Hegab HA, Darras B, Kishawy HA. Towards sustainability assessment of machining processes. J Clean Prod 2018;170:694–703. https://doi.org/10.1016/j.jclepro.2017.09.197.

[2] Vogtel P, Klocke F, Lung D. High performance machining of profiled slots in nickel-based-superalloys. Procedia CIRP 2014;14:54–9. https://doi.org/10.1016/j.procir.2014.03.061.

[3] Zhu D, Zhang X, Ding H. Tool wear characteristics in machining of nickel-based superalloys. Int J Mach Tool Manufact 2013;64:60–77. https://doi.org/10.1016/j.ijmachtools.2012.08.001.

[4] Costes JP, Guillet Y, Poulachon G, Dessoly M. Tool-life and wear mechanisms of CBN tools in machining of Inconel 718. Int J Mach Tool Manufact 2007;47:1081–7. https://doi.org/10.1016/j.ijmachtools.2006.09.031.

[5] Brandt G, Gerendas A, Mikus M. Wear mechanisms of ceramic cutting tools when machining ferrous and non-ferrous alloys. J Eur Ceram Soc 1990;6:273–90. https://doi.org/10.1016/0955-2219(90)90019-C.

[6] Erdemir A, Donnet C. Tribology of diamond-like carbon films: recent progress and future prospects. J Phys D Appl Phys 2006;39:R311–27. https://doi.org/10.1088/0022-3727/39/18/R01.

[7] Folea M, Roman A, Lupulescu N-B. An overview of DLC coatings on cutting tools performance. Acad J Manuf Eng 2010;8:30–6.

[8] Boughdiri I, Giasin K, Mabrouki T, Zitoune R. Effect of cutting parameters on thrust force, torque, hole quality and dust generation during drilling of GLARE 2B laminates. Compos Struct 2021;261:113562. https://doi.org/10.1016/j.compstruct.2021.113562.

[9] Konca E, Cheng Y-T, Alpas AT. Dry sliding behaviour of non-hydrogenated DLC coatings against Al, Cu and Ti in ambient air and argon. Diam Relat Mater 2006;15:939–43. https://doi.org/10.1016/j.diamond.2005.11.030.

[10] Evaristo M, Fernandes F, Cavaleiro A. Room and high temperature tribological behaviour of W-DLC coatings produced by DCMS and hybrid DCMS-HiPIMS configuration. Coatings 2020;10:319. https://doi.org/10.3390/coatings10040319.

[11] Tobola D, Liskiewicz T, Yang L, Khan T, Boroń Ł. Effect of mechanical and thermochemical tool steel substrate pre-treatment on diamond-like carbon (DLC) coating durability. Surf Coat Technol 2021;422:127483. https://doi.org/10.1016/j.surfcoat.2021.127483.

[12] Khan SA, Ferreira F, Oliveira J, Emami N, Ramalho A. A comparative study in the tribological behaviour of different DLC coatings sliding against titanium alloys. Wear 2024;554–555:205468. https://doi.org/10.1016/j.wear.2024.205468.

[13] Rajak DK, Kumar A, Behera A, Menezes PL. Diamond-like carbon (DLC) coatings: classification, properties, and applications. Appl Sci 2021;11:4445. https://doi.org/10.3390/app11104445.

[14] Ferrari AC, Robertson J. Interpretation of Raman spectra of disordered and amorphous carbon. Phys Rev B 2000;61:14095–107. https://doi.org/10.1103/PhysRevB.61.14095.

[15] Buyanovskii IA, Khrushchov MM, Samusenko VD. Tribological behavior of diamond-like carbon coatings under boundary friction: Part I. Structure, testing methods, lubrication by adsorption layers. Inorg Mater: Appl Res 2022;13:893–906. https://doi.org/10.1134/S2075113322040086.

[16] Sutton DC, Limbert G, Stewart D, Wood RJK. The friction of diamond-like carbon coatings in a water environment. Friction 2013;1:210–21. https://doi.org/10.1007/s40544-013-0023-1.

[17] Hagarová M, Baranová G, Heželová M, Truchlý M, Vojtko M, Petruš O, Csík D. High-temperature mechanical and tribological performance of W-DLC coating with Cr interlayer on X40CrMoV5-1 hot work tool steel. Coatings 2024;14:971. https://doi.org/10.3390/coatings14080971.

[18] Banerji A, Bhowmick S, Alpas AT. High temperature tribological behavior of W containing diamond-like carbon (DLC) coating against titanium alloys. Surf Coat Technol 2014;241:93–104. https://doi.org/10.1016/j.surfcoat.2013.10.075.

[19] Hofmann D, Kunkel S, Bewilogua K, Wittorf R. From DLC to Si-DLC based layer systems with optimized properties for tribological applications. Surf Coat Technol 2013;215:357–63. https://doi.org/10.1016/j.surfcoat.2012.06.094.

[20] Angus JC. Diamond and diamond-like films. Thin Solid Films 1992;216:126–33. https://doi.org/10.1016/0040-6090(92)90881-B.

[21] Holmberg K, Ronkainen H, Laukkanen A, Wallin K. Friction and wear of coated surfaces — scales, modelling and simulation of tribomechanisms. Surf Coat Technol 2007;202:1034–49. https://doi.org/10.1016/j.surfcoat.2007.07.105.

[22] Zhendong L, Hua Z, Tianyang X, Manyu B, Bihan L, Ruijun W. Influence of Cr interlayer thickness on residual stress and adhesion of Cr-DLC multilayer structure films. Rare Met Mater Eng 2022;51:1195–202.

[23] Freund L Ben, Suresh S. Thin film materials: stress, defect formation and surface evolution. Cambridge university press; 2004.

[24] Hauert R. A review of modified DLC coatings for biological applications. Diam Relat Mater 2003;12:583–9. https://doi.org/10.1016/S0925-9635(03)00081-5.

[25] Shu C, Yin S, Huang S. Preparation and performance of Ti/Ti-DLC composite coatings for precision glass molding. Ceram Int 2024;50:5210–23. https://doi.org/10.1016/j.ceramint.2023.11.267.

[26] van der Kolk GJ. Wear resistance of amorphous DLC and metal containing DLC in industrial applications. In: Tribology of diamond-like carbon films. Boston, MA: Springer US; 2008. p. 484–93. https://doi.org/10.1007/978-0-387-49891-1_19.

[27] Klocke F, Lung D, Buchkremer S. Inverse identification of the constitutive equation of Inconel 718 and AISI 1045 from FE machining simulations. Procedia CIRP 2013;8:212–7. https://doi.org/10.1016/j.procir.2013.06.091.

[28] Wang L, Liu Y, Chen H, Wang M. Modification methods of diamond like carbon coating and the performance in machining applications: a review. Coatings 2022;12:224. https://doi.org/10.3390/coatings12020224.

[29] Sharifahmadian O, Pakseresht A, Amirtharaj Mosas KK, Galusek D. Doping effects on the tribological performance of diamond-like carbon coatings: a review. J Mater Res Technol 2023;27:7748–65. https://doi.org/10.1016/j.jmrt.2023.11.132.

[30] Fernandes F, Ramalho A, Loureiro A, Cavaleiro A. Mapping the micro-abrasion resistance of a Ni-based coating deposited by PTA on gray cast iron. Wear 2012;292–293:151–8. https://doi.org/10.1016/j.wear.2012.05.018.

[31] Fernandes F, Calderon VS, Ferreira PJ, Cavaleiro A, Oliveira JC. Low peak power deposition regime in HiPIMS: deposition of hard and dense nanocomposite Ti-Si-N films by DOMS without the need of energetic bombardment. Surf Coat Technol 2020;397:125996. https://doi.org/10.1016/j.surfcoat.2020.125996.

[32] Kameneva A, Kichigin V, Bublik N. Structure and electrochemical behavior of AlN, AlTiN, and AlTiSiN physical vapor deposition coatings in 3% NaCl solution. J Mater Eng Perform 2022;31:10402–11. https://doi.org/10.1007/s11665-022-07030-w.

[33] Evaristo M, Fernandes F, Cavaleiro A. Influence of the alloying elements on the tribological performance of DLC coatings in different sliding conditions. Wear 2023;526–527:204880. https://doi.org/10.1016/j.wear.2023.204880.

[34] Zhang S, Huang T, Sun S, Wu S, Yang X, Guo F, Zhang B, Dai L. Effects of bias voltages on the tribological behaviors of DLC coatings. Coatings 2024;14:176. https://doi.org/10.3390/coatings14020176.

[35] Sheng H, Xiong W, Zheng S, Chen C, He S, Cheng Q. Evaluation of the sp3/sp2 ratio of DLC films by RF-PECVD and its quantitative relationship with optical band gap. Carbon Lett 2021;31:929–39. https://doi.org/10.1007/s42823-020-00199-x.

[36] Moolsradoo N, Abe S, Watanabe S. Thermal stability and tribological performance of DLC-Si–O films. Adv Mater Sci Eng 2011;2011:1–7. https://doi.org/10.1155/2011/483437.

[37] Bakdemir SA, Özkan D, Türküz MC, Salman S. A study on the effect of AlTiN and TiCN coatings on the tribological properties of dental drills. In: Advanced ceramic coatings for emerging applications. Elsevier; 2023. p. 265–89. https://doi.org/10.1016/B978-0-323-99624-2.00012-7.

[38] Tillmann W, Grisales D, Stangier D, Thomann C-A, Debus J, Nienhaus A, Apel D. Residual stresses and tribomechanical behaviour of TiAlN and TiAlCN monolayer and multilayer coatings by DCMS and HiPIMS. Surf Coat Technol 2021;406:126664. https://doi.org/10.1016/j.surfcoat.2020.126664.

[39] Ferreira F, Serra R, Cavaleiro A, Oliveira J. Diamond-like carbon coatings deposited by deep oscillation magnetron sputtering in Ar-Ne discharges. Diam Relat Mater 2019;98:107521. https://doi.org/10.1016/j.diamond.2019.107521.
[40] Jiang J, Arnell RD. The effect of substrate surface roughness on the wear of DLC coatings. Wear 2000;239:1–9. https://doi.org/10.1016/S0043-1648(99)00351-8.
[41] Lafer S.p.A.: AlTiSiN multi-layer coating, https://www.lafer.eu/coating-technology/?lang=en, last accessed 2024/09/12.
[42] Wu W-J, Hon M-H. Thermal stability of diamond-like carbon films with added silicon. Surf Coat Technol 1999;111:134–40. https://doi.org/10.1016/S0257-8972(98)00719-1.
[43] Evaristo M, Azevedo R, Palacio C, Cavaleiro A. Influence of the silicon and oxygen content on the properties of non-hydrogenated amorphous carbon coatings. Diam Relat Mater 2016;70:201–10. https://doi.org/10.1016/j.diamond.2016.10.024.
[44] Das A, Kamal M, Das SR, Patel SK, Panda A, Rafighi M, Biswal BB. Comparative assessment between AlTiN and AlTiSiN coated carbide tools towards machinability improvement of AISI D6 steel in dry hard turning. Proc Inst Mech Eng C J Mech Eng Sci. 2022;236:3174–97. https://doi.org/10.1177/09544062211037373.
[45] Das A, Kumar A, Padhan S, Das SR, Satpathy MP, Patel SK. Hard turning of AISI H10 steel using AlTiN and AlTiSiN coated carbide tools: comparative machining performance evaluation and economic assessment. J Braz Soc Mech Sci Eng 2024;46:277. https://doi.org/10.1007/s40430-024-04855-5.
[46] Miletić A, Panjan P, Škorić B, Čekada M, Dražič G, Kovač J. Microstructure and mechanical properties of nanostructured Ti–Al–Si–N coatings deposited by magnetron sputtering. Surf Coat Technol 2014;241:105–11. https://doi.org/10.1016/j.surfcoat.2013.10.050.
[47] Liang J, Almandoz E, Ortiz-Membrado L, Rodríguez R, de Ara JF, Fuentes GG, Llanes L, Jiménez-Piqué E. Mechanical performance of AlCrSiN and AlTiSiN coatings on Inconel and steel substrates after thermal treatments. Materials 2022;15:8605. https://doi.org/10.3390/ma15238605.
[48] Getachew BA, Wang T-G. Effect of modulation period on the structure and properties of AlTiN/AlTiSiN multilayers. Int. Res. J. Eng. Technol. 2020;9:62–8.
[49] Ling ZP, Ge J, Stangl R, Aberle AG, Mueller T. Detailed micro Raman spectroscopy analysis of doped silicon thin film layers and its feasibility for heterojunction silicon wafer solar cells. J Mater Sci Chem Eng 2013;1:1–14. https://doi.org/10.4236/msce.2013.15A001.
[50] Vink RLC, Barkema GT, van der Weg WF. Raman spectra and structure of amorphous Si. Phys Rev B 2001;63:115210. https://doi.org/10.1103/PhysRevB.63.115210.